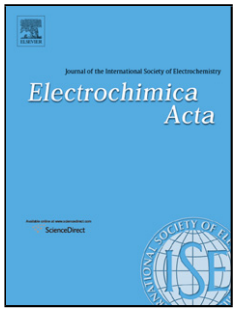

Title: NiO hollow microspheres interconnected by carbon nanotubes as an anode for lithium ion batteries

Author: Wen Cao Aiping Hu Xiaohua Chen Xiaohong Liu Peng Liu Qunli Tang X.S. Zhao

PII: S0013-4686(16)31600-0
DOI: http://dx.doi.org/doi:10.1016/j.electacta.2016.07.094
Reference: EA 27709

To appear in: *Electrochimica Acta*

Received date: 11-6-2016
Revised date: 15-7-2016
Accepted date: 17-7-2016

Please cite this article as: Wen Cao, Aiping Hu, Xiaohua Chen, Xiaohong Liu, Peng Liu, Qunli Tang, X.S.Zhao, NiO hollow microspheres interconnected by carbon nanotubes as an anode for lithium ion batteries, Electrochimica Acta http://dx.doi.org/10.1016/j.electacta.2016.07.094

NiO hollow microspheres interconnected by carbon nanotubes as an anode for lithium ion batteries

Wen Cao[a], Aiping Hu[a,b*], Xiaohua Chen[a*], Xiaohong Liu[a], Peng Liu[b], Qunli Tang[a], X. S. Zhao[b]

[a]*College of Materials Science and Engineering, Hunan Province Key Laboratory for Spray Deposition Technology and Application, Hunan University, Changsha 410082, China*

[b]*School of Chemical Engineering, The University of Queensland, St. Lucia, Brisbane, QLD 4072, Australia*

[*]Corresponding author: aipinghu@hnu.edu.cn (Aiping Hu); xiaohuchen@hnu.edu.cn (Xiaohua Chen)

Abstract

In this work, NiO hollow microspheres interconnected by multi-walled carbon nanotubes (MWCNTs) were prepared, characterized, and evaluated in terms of lithium ion storage properties. Characterization results showed that the NiO hollow microspheres were formed by self assembly of NiO nanoparticles promoted by MWCNTs, which connected the NiO microspheres to form a long-range network. Electrochemical measurement results showed a charge capacity as high as 597.2 mAh g^{-1} when cycling at the rate 2C and maintained 85.3% capacity of 0.1C. After cycling for 100 times at 1C, it maintained a capacity of 692.3 mAh g^{-1} with retention 89.3% of the initial capacity. The observed excellent electrochemical performance is attributed to the presence of MWCNTs interconnecting the NiO microspheres of the composite material, of which electronic conductivity was improved, and the mesoporous hollow structure effectively alleviated the volume changes to maintain the structural stability during cycling.

Keywords: NiO/CNTs; nanoparticle clusters; long-range conductive networks; hollow microsphere; lithium-ion batteries

1. introduction

With the extensive applications of lithium-ion batteries (LIBs) to consumer electronics and electric vehicle, high performance electrode materials with high energy, high power densities and good cycle stability should be developed[1]. In the recent two decades, some transition metal oxides (MO) such as Co_3O_4, NiO have been extensively investigated as potential anodes for LIB due to their high capacity, abundance, and low cost[2, 3]. However,

*Corresponding author: aipinghu@hnu.edu.cn (Aiping Hu); xiaohuchen@hnu.edu.cn (Xiaohua Chen)

they suffered from fast capacity decay and poor rate performance, which mainly resulted from the large volume change and their poor electrical conductivity during discharging/charging cycles, respectively. Up to now, it has been widely demonstrated that these obstacles could be partly solved by building porous nanostructure because the porosity could not only alleviate the strain of volume change to keep the stability of metal oxide electrode, but also shorten the transport distance of electrons and ions to improve the rate performance during cycles[3-7]. Unfortunately, due to its high surface area, thick and wide range of solid electrolyte interphase (SEI) films on the electrode surface would form during cycles, which can consume some Li^+ supplied by the cathode, leading to a low columbic efficiency and a high level irreversibility loss of capacities. In order to further solve this problem, much effort has been developed to build a core-shell structure such as C@MO because the SEI films being formed on the surface of coated carbon are relatively stable and intense so that it can act as a protective layer to improve the columbic efficiency and make the electrode show high cycling stability [8-10]. However, due to the coated carbon tightly wrapping the surface of the active materials, the large strain caused by volume effect cannot effectively alleviate. More unfortunately, generally, the coated amorphous carbon obtained by heat decomposition methods showed a low graphitization degree and often exhibited poor electrical conductivity, leading to the unsatisfied rate performance of the electrode. Therefore, it is still a challenge to improve the comprehensive electrochemical properties of metal oxide active materials.

To further improve the rate performance of MOs, much effort has been made to accommodate the active materials with porous conductive scaffolds to form the nanocomposites such as carbon nanotubes[11-19], graphene[20-24] and carbon nanofibers[25-29] because they could provide long-range conductivity, well controlled interface between MOs and conducting carbons, and more robust network structure. In

particular, CNTs is a good candidate for a support matrix in novel anode material for enhanced lithium storage due to its high electrical conductivity, rich porosity and high tensile strength[30, 31]. Most importantly, CNTs allows for lower weight doping levels to achieve a comparable percolation threshold due to its high aspect ratio and excellent electrical conductivity [32]. Therefore, as an additive, it is more beneficial to effectively obtain the high capacity of MO composites electrode with excellent rate performance. To date, CNTs /MO composites mainly include three kinds of structures: (1) core-shell CNTs structure with metal oxide particles depositing on the surface of CNTs[11, 15]; (2) the interpenetrating structures with metal oxide 1D nanostructures intertwining within CNTs[33]; (3) the integrated structure of MO active materials penetrated with CNT networks[19, 34]. In the first structure, active material particles mainly anchored on the surface of CNTs and its content in the composites is not enough to obtain high specific capacity. In addition, it only makes effective transfer of charges locally because of the insulated SEI film being formed during cycles. In the second structure, it could provide not only enough space to alleviate the stress resulted from volume change during the repeated Li^+ uptake/release but also better long-range conductivity in the electrodes. Unfortunately, it suffered from loose interfacial contact between 1D metal oxides and showed poor structural integrity. Generally, the third composites could show intimate interfacial contacts and robust structural integrity so that it was expected to show excellent electrochemical performance. For example, X. Jia et al built CNTs interweaved Fe_3O_4 nanocrystal architecture by spray drying process with PEO as surfactant. When cycled at 12C, it still retained 45% capacity at 0.1C [34].

Herein, we obtained a structure of NiO hollow microspheres penetrated with CNTs by a facile ultrasonication-assisted method without adding any surfactant. The design of this structure was based on the following considerations: (1) CNTs not only embedded in the microspheres but also bridged NiO microspheres to form long-range 3D conducting networks

so as to ensure the excellent rate performance of the integral electrode; (2) the microspheres consisting of nanoparticles with rich pores, and the coated carbon layer on the surface of NiO can promote the formation of stable SEI films to improve the cycle stability of the electrode; (3) the hollow structure can not only well accommodate volume change during cycles to improve the cycling property, but also provide more lithium-storage sites to improve the specific capacities. In this structure, the composite combines the advantages of high capacity of NiO active materials and the high conductivity of CNTs, as well as the structure advantages of nanoparticles second structure, reasonable porosity and core-shell structure. Therefore, it is expected to show excellent electrochemical performances for LIBs.

2. Experimental

2.1 Synthesis of samples

All chemical agents were analytical grade and used without further purification. Multiwalled Carbon nanotubes (MWCNTs) were purchased from Beijing CNano Technology Limited.

(1) The functionalization of CNTs. 15 ml HNO_3 (concentrated nitric acid 65%), 45ml H_2SO_4 (concentrated sulfuric acid 98%) and 100 mg MWCNTs were mixed in a flask, and then ultra-sonicated for 120 min. The resulting mixture was centrifuged and washed repeatedly with distilled water until the filtrate with neutral pH value. The functionalized resultant CNTs were homogeneously dispersed in distilled water.

(2) Preparation of samples. In a typical procedure, NiO/CNTs hollow microspheres were prepared by a facile two-step method. Firstly, 15ml functionalized MWCNTs was ultrasonicated and then added into 50 mL 0.2 M $Ni(NO_3)_2$ solution by magnetic stirring for 10 mins. Subsequently, 100 mL 0.1 M $(NH_4)_2C_2O_4$ solution was quickly added. After the mixed solution was stirred for 5 min, it was kept under sonication at room temperature for 40

min. The resultant grey precipitate was centrifuged and washed with distilled water and absolute ethanol until the pH of the filtrate was about 7. Secondly, after it was dried at 60 ˚C for 12 h, the precursor was transferred into a quartz boat and heat-treated at 380 ˚C for 30 min in a tubular furnace with a heating rate of 3 °C min^{-1} in the atmosphere. For comparison, pure NiO sample was also prepared by the same process without CNTs.

2.2 Characterization

The phases of the products were characterized by X-ray powder diffraction (XRD, Siemens D5000 X-ray diffractometer with Cu·Kα, λ=0.15406 nm, 40 kV, and 50 mA). The morphology and structures of samples were observed by field emission scanning electron microscopy on a Hitachi S-4800 microscope at 5kV and transmission electron microscopy (TEM) was obtained with a JEM-2010F system operated at 200kV. FT-IR spectra were recorded on a Nicolet 6700 FT-IR spectrometer (Thermo Electron Scientific Instruments, U.S.). Thermogravimetric analysis (TGA) was carried out on a TG/DTA 7300 thermal analyzer with a heating rate of 5 °C min^{-1} in air from room temperature to 850°C. The BET surface area and pore size distributions were determined by N_2 adsorption in a Micromeritics Tristar II 3020 sorptometer.

2.3 Electrochemical measurements

Electrochemical experiments were carried out by CR2032-type coin cells. The working electrodes were prepared by a mixture of active material (NiO or NiO/CNTs nanocomposites), acetylene black, and sodium carboxymethylcellulose (CMC) at a weight ratio of 80:10:10, dispersed in distilled water to form a slurry. The slurry was uniformly spread on Cu foil with a blade and dried at 120 °C in a vacuum oven. Model cells were fabricated with lithium foil as counter electrode and a solution of 1 M$LiPF_6$ in ethylene carbonate (EC)/dimethyl carbonate (DMC)/diethyl carbonate (DEC) (1:1:1,wt.%) as the electrolyte. The CR2032-type coin cells were assembled in an argon-filled glove box. Galvanostatic cycling experiments

were performed on a Land CT2001A battery test system in the voltage range 0.01–3.00 V versus Li^+/Li at 25 °C. The total mass of the composites was included when the current density was calculated.

3. Results and discussion

Fig. 1A shows the X-ray diffraction (XRD) patterns of the composites, the sample prepared without CNTs and the functionalized CNTs. The diffraction peaks of two curves (a) and (b) can be assigned to nickel oxide (NiO) (JCPDS Card No. 47−1049). The peaks at 44.507, 51.846 and 62.878 degree correspond to the (111), (200) and (220) plane of NiO, respectively. In the Fig.1A(c), the wide diffraction peak at 25.9 degree corresponds to the (002) of functionalized CNTs, which is consistent with the reported result [35]. It indicates that the integral structure of CNTs keeps orderly although their surfaces are partly modified by some oxygen-containing groups, which can make sure that CNTs effectively play the role of excellent electric conductor in the NiO/CNTs composites. However, it is not clearly found the diffraction peaks of carbon in Fig.1A(a) and (b), which may be due to the low content of CNTs and disorder of amorphous carbon in the samples.

In order to determine the amount of components in the NiO/CNTs nanocomposites, TG measurement was performed. Fig. 1B shows the weight loss during a heat-treatment from room temperature up to 850 ^oC with a heating rate of 10 ^oC/min in air atmosphere. The initial mass loss 1% at lower temperature is mainly due to the release of water, and then the another mass loss 1% less than 450^oC resulted from the oxidation of amorphous carbon [36-38]. A sharp loss in mass is observed between 450^oC and 670^oC, which is attributed to the oxidation of CNTs. Based on the analysis above, the mass ratio of NiO, CNTs and amorphous carbon in NiO/CNTs hollow microspheres is about 91%, 8% and 1%, respectively.

Representative images of scanning electron microscope (SEM) for NiO/CNTs sample are shown in Fig. 2a, b. As can be seen from Fig.2a, the sample consists of a large quantity of monodispersed microspheres. In addition, some broken spheres could also be observed, confirming that spheres have a hollow interior. From the magnified image (Fig.2b), it can further be known that microspheres are composed of closely attached nanopariticles. Importantly, carbon nanotubes not only disperse in the microspheres, but also extrude out to bridge microspheres, which can effectively solve the electric conductivity issue between microspheres associated with the insulated SEI so as to improve the long-range electronic conductivity of this sample. From the transmission electronmicroscopy (TEM, Fig.2c), it can be found that the microspheres are made up of networks of NiO nanoparticles with CNTs penetrating through them. The high-resolution TEM image in Fig. 2d shows the lattice fringes of the nanocrystallite with a d-spacing of 0.24 nm, which can be assigned to the (111) plane of NiO. Notably, the surfaces of NiO microspheres are coated with the amorphous carbon , which can not only provide the space to alleviate the strain of volume change but also protect the internal active material nanoparticles from agglomerating to improve the cycle stability. The corresponding ringlike selected-area electron diffraction (SAED) pattern (inset in Fig. 2d) indicates that the nanostructures are polycrystalline.

The FT-IR spectra of functionalized CNTs, NiO, and NiO/CNTs were presented in Fig. 3. Functionalized CNTs were obtained through oxidation of carbon nanotubes by concentrated nitric acid and sulfuric acids. Its representative peaks confirmed the presence of the oxygen-containing functional groups (C–O–C , -COOH, -OH) in carbon frameworks, including bands at 1056cm^{-1} (C–O stretching vibration of epoxide), 1700 cm^{-1} (C=O stretching of carbonyl groups)[39] and 1644 cm^{-1} (-O-H bending vibration), as well as absorption band was observed at 1565 cm^{-1}, which can be attributed to the aromatic skeletal C=C stretching vibration of CNTs[40]. This result revealed that some portion of C=C bonds

were oxidized to hydroxyl, carboxyl and epoxy groups，and some of them remained in the CNTs, which not only could make CNTs easily absorb Ni^{2+} ions through electrostatic interaction to form composites but also ensure the excellent electrical conductivity of CNTs. In comparison, in the FT-IR spectrum of the NiO/CNTs sample (Fig. 3c), the peaks of CNTs at 1700 cm^{-1} vanished, which should be resulted from thermal decomposition of carboxyl group. Notably, the peak intensity of Ni-O bonds at 549cm^{-1} and 1484cm^{-1} in the curve of NiO/CNTs becomes weaker than that of pure NiO sample. It indicates that some Ni atoms bond with CNTs in NiO/CNTs nanocomposites, which makes it possible for the NiO nanoparticles to firmly anchor on the surface of CNTs through covalent bonds.

To further determine the specific surface area and porosity of the hollow microspheres, N_2 adsorption/desorption isothermal analysis and the relative BJH pore size distribution curves of NiO/CNTs and NiO samples were carried out, as shown in Fig. 4. Obviously, both N_2 adsorption-desorption isotherms can be indexed to type IV with a hysteresis loop in the range of 0.5–0.98 P/P_0, which suggests that rich mesoporous structure exist in both samples. In addition, it can be known that NiO/CNTs hollow microspheres has Brunauer−Emmett−Teller (BET) surface area of 87.40 m^2/g and the total pore volume of 0.24cm^3/g, much higher than those of NiO hollow microspheres for 61.96 m^2/g and 0.15 cm^3/g, respectively. From their pore distribution profiles (the insets in Fig. 4a and Fig. 4b), it can be seen that NiO/CNTs and NiO samples have a main pore distribution from 2 to 10 nm, which further confirms that the rich mesoporous structure exist in two samples. The richer pores of NiO/CNTs microspheres mainly come from not only the space between NiO nanoparticles, and the gap between NiO and CNTs, but also the loose amorphous carbon shell coating on the surface of NiO and hollow structure. The abundant mesopores can facilitate the electrolyte smoothly to the active materials as well as provide sufficient void spaces to accommodate large volume expansion and contraction during discharging/charging cycles.

To investigate the mechanism of NiO/CNTs hollow spheres, some condition experiments were carried out. Firstly, the well dispersion of CNTs in the aqueous solution is an important factor to form the CNTs homogeneously penetrated electrical conductive network of NiO spheres. Secondly, the precipitation agent for Ni^{2+} plays a key role in the formation of hollow spheres. It can be obviously seen from Fig. S1, (Supporting Information) when ammonium oxalate, sodium carbonate, sodium hydrate and urea were used as the precipitation agent, respectively, hollow microspheres can be obtained only with ammonium oxalate. According to the experimental results above, the synthetic procedure for the NiO/CNTs hollow microspheres is schematically illustrated in Fig.5. (1) Through CNTs being refluxed with the mixture of nitric acid and sulfuric acid, the impurities of raw CNTs(Fig. 5a) were removed and they were modified with abundant oxygen-containing functional groups such as C–O–C , -COOH, -OH (Figure 5b), which was confirmed by the FT-IR (Fig. 3). In the synthesis procedure, these modified groups of CNTs play important roles as follows: (i) the wettability of these groups promotes CNTs to disperse well in the aqueous solution; (ii) nickel ions could be homogeneously and tightly connected with CNTs through the electrostatic interaction between the strongly negatively charged carboxyl groups of CNTs and nickel ions, as well as covalent bonds between the hydryl group, epoxy group and nickel ions. As long as the oxygen-containing functional groups on the surface of CNTs are enough, CNTs could disperse well in water and effectively adsorb the Ni^{2+} cations, which ensure the CNTs evenly penetrating into the NiO microspheres to form excellent conductive network. (2) When the well dispersed CNT suspension was added into the nickel dichloride solution (Fig. 5c), Ni^{2+} cations were adsorbed on the surface of CNTs and then reacted with $C_2O_4^{2-}$ anions to form NiC_2O_4 nanoparticles (Fig. 5d). They grow and then self-assemble into solid microspheres (Fig. 5e) under ultrasonication. (3) Finally, by annealing treatment, nickel oxalate hydrates ($NiC_2O_4.2H_2O$) were decomposed to water vapour, amorphous carbon and

some CO_2 in the air atmosphere, and were converted to NiO nanoparticles to self-assemble porous NiO hollow microspheres. The formation of porous hollow microspheres should be attributed to the combined effect generated by the oxidative decomposition of the precursor, contraction of the particle framework, and the simultaneous gas evacuation during heat treatment[3]. Particularly, the precursor plays an important role in the formation of hollow structure. NiC_2O_4 can be decomposed to form the hollow structure but $Ni(OH)_2$, $NiCO_3$ cannot, which is attributed to the fact that NiC_2O_4 can release more H_2O, CO_2 and carbon to form richer pores in the NiO framework than any other precipitator.

In order to study the electrochemical properties of NiO/CNTs microspheres, the CR2032 coin cells with metallic lithium counter electrode were assembled and evaluated. The typical charge/discharge curves of NiO/CNTs microspheres electrode for the first three cycles at a current density of 0.1C are shown in Fig.7a. In the first discharge voltage profile, it exhibits a long voltage plateau at about 0.75V, corresponding to the electrochemical reaction $NiO+2Li^+ \rightarrow Ni+Li_2O$ to form Ni^0. The initial discharge capacity of 930 mA h g^{-1} is higher than the theoretical capacity of NiO (723 mA h g^{-1}). This extra specific capacity may be attributed to the adsorption of Li^+ through the cation vacancies of metal oxide hollow spheres[41, 42], the surface of porous CNTs and coated carbon in the microspheres[43, 44]. In the first charge process, an overall specific charge capacity of 700 mA h g^{-1} was delivered, corresponding to the first columbic Efficiency of 75.2%. The second discharge profile shows a higher plateau voltage than the first cycle, which suggests drastically structural or textural modifications[45]. Importantly, the discharge/charge curves for the second and third cycles almost overlap, indicating the excellent cycling stability of NiO/CNTs electrode.

Fig.6 shows the typical cyclic voltammogram (CV) curves of the NiO/CNTs microspheres and NiO sample in the potential range of 0.01-3.00V with a constant scan rate of 0.1mV S^{-1}. It can be found that the CV curve of the NiO/CNTs microspheres is similar to

that of NiO. In the first cycle, there are two obvious reduction peaks at about 0.95V and 0.55V, which is similar with the previous study[46]. The peak at 0.95V could be attributed to the conversion of NiO to Ni, and the peak at 0.55V should be resulted from the formation of SEI films. In the first oxidation process, two peaks were recorded at 1.40V and 2.19V, which correspond to the dissolution of the organic SEI film[47], and the charge reaction $Ni + Li_2O \rightarrow NiO + 2Li$, respectively [5]. The CV curves in the subsequent two cycles almost overlap, which matches well with the result of previous discharge/charge voltage profiles, indicating excellent stable cycle reversibility of the work electrode. Furthermore, after the first cycle, the reduction peak positively shifts to 1.1V or so, which is consistent with the result of previous voltage profile. Moreover, from the CV curve of NiO/CNTs composite, it cannot be obviously found the reduction peak of carbon, which illustrates that the active material is mainly NiO in the composite electrode.

To investigate the rate performance, the specific capacity curves of NiO/CNTs nanocomposites and NiO electrodes were evaluated between 0.01 and 3.0 V at the rate of 0.1 C-5 C (1 C=723 mAh/g) for 10 times, respectively. The results were shown in Fig. 7b. The charge capacity of NiO/CNTs nanocomposites of 700 mA h g^{-1} is achieved at the rate 0.1 C. At current rates of 0.2 C, 0.5 C, 1 C, 2 C, and 5 C, it still retains high reversible specific capacities of 757.0 mAh/g, 739.2 mAh/g, 656.2 mAh/g, 597.2 mAh/g and 493.2 mAh/g, respectively, 108.1%, 105.6%, 93.7%, 85.3% and 70.5% of the capacity at 0.1C, respectively. In contrast, the charge capacities of pure NiO sample at 0.2C, 0.5C, 1C, 2C and 5C are 852.2 , 855.3，797.2，653.2，409.6 mAh/g, retention of 115.9%, 116.3%, 108.4%，88.9%，55.7% capacity at 0.1C, respectively. When cycled at low current rate in the range from 0.1C to 2C, NiO/CNTs exhibit less specific capacities than NiO, which results from the low specific capacity of the CNTs in the nanocomposites. However, the degree of its specific decay is less than that of NiO electrode. Notably, when at the rate 5C, the NiO/CNTs electrode shows

higher specific capacities than NiO. It retains 70.5% of initial capacity, much higher than pure NiO electrode of only 55.7%. Apparently, the NiO/CNTs electrode shows superior rate performance than NiO sample, and also better than the reported results in the literatures [3, 5, 48, 49]. In addition, the specific capacity increase at low rate (0.1C,0.2C and 0.5C) and decrease at high rate (1C, 2C and 5C). It might be the result of two factors as follows: on the one hand, its specific capacity increases due to the activation process of the electrode during cycles[50-52]; on the other hand, metal oxides suffer from sluggish kinetics owing to their poor conductivity, the capacity would decrease with the increase of current rate; when the working electrode cycling at a low rate, the activation process is more dominant than the kinetic effects, which leads to the higher capacities; with the current rate further increasing, the polarization of electrode occupies a leading position, which causes the specific capacity to decrease at higher rate.

From the columbic efficiency profiles of NiO/CNTs and NiO electrode in Fig.7b, it can be seen that when discharging/charging in the turning cycle from low to high current rate, namely, at 11^{th}, 21^{th}, 31^{th}, 41^{th}, 51^{th} cycle, the columbic efficiencies of NiO/CNTs and NiO are 96.6%, 96.6%, 96.7%, 96.3%, 94.3% and 97.7%, 97.1%, 95.9%, 93.9% and 90.3% respectively. NiO/CNTs and NiO electrodes both show similar high columbic efficiencies of more than 96.0% at low rates. However, at high current rates, NiO/CNTs electrode exhibits higher columbic efficiency than pure NiO electrode. For example, when cycling at the current rate from 2C to 5C, the columbic efficiencies of NiO/CNTs and NiO electrode are 94.3% and 90.3%, respectively. It suggests that NiO/CNTs electrode can run the electrochemical reversal reaction more effectively and shows less decay of specific capacities than the NiO electrode, which can be ascribed to the fact that penetrated CNTs in the NiO hollow porous sphere have formed the excellent integral conductive network and make the electrons and ions transport smoothly in active materials.

Electrochemical impedance spectroscopy (EIS) measurements were carried out to investigate the effect of CNTs penetrating in the nanocomposites on the electronic conductivity. The Nyquist plots of NiO/CNTs and NiO electrodes after 50 cycles are shown in Fig.7c. The plots display a semicircle in the high-middle frequency region, being assigned to the charge transfer resistance, and a sloping straight line in the low-frequency range, which represents the Warburg impedance[53]. It can be obviously seen that the diameter of semicircle for NiO/CNTs is smaller than that of NiO electrode, which indicates that the electrons and lithium ions transport more smoothly in NiO/CNTs electrode. This result is consistent with the superior rate performance and the higher columbic efficiency of NiO/CNTs than NiO electrode.

The cycling performances of NiO/CNTs and NiO electrodes were tested between 0.01V and 3V for 100 cycles at a current density of 723 mA/g (1C), as shown in Fig.7d. The NiO/CNTs electrode delivered a high charge capacity of 774.9 mAh g^{-1} and maintained a capacity of 692.3 mAh g^{-1} after 100 cycles with 89.3% retention of the initial capacity. In comparison, although the NiO electrode shows an outstanding initial discharge capacity of 801.9 mAh g^{-1}, it decreases dramatically to only 549.3 mAh g^{-1} after 100 cycles with poor capacity retention of 68.5%. Obviously, NiO/CNTs electrode shows a better cycle stability than NiO, which is mainly due to its more abundant porous structure to alleviate the strains associated with the volume change during cycles. As similar as the result of Fig.7b, with the cycles going on, the specific capacities gradually increase and then decrease slowly. The increased capacities are owing to the activation process of the electrode. The decay of capacities might be resulted from the slight volumn change of active materials and the irreversible capacity loss which can be demonstrateded by the columbic efficiency data in Fig.7d.

From the columbic efficiency profile in Fig.7d, the first columbic efficiency of NiO/CNTs is 70.0%, slightly less than NiO, which results from its higher specific surface and need more Li ions to form SEI films. From the second cycle, the columbic efficiencies of the electrode are more than 97.0%, which indicates the excellent reversibility of the electrodes. It is attributed to the formation of stable SEI films during cycles due to the microsphere composed of nanoparticles second structure [46] and the coated amorphous carbon.

To further confirm the robust structure of NiO/CNTs microshperes, the morphology of working electrode material after 100 cycles at a current rate 1C was examined under scanning electron microscopes. As shown in Fig.8, the microsphere structure can be found in the image, which indicates that the active materials maintain its structural stability on the whole during cycles. This should be attributed to the rich mesoporous hollow structure to accommodate the large volume change during discharging/charging reaction and alleviate the pulverization process so as to assure the stable cycling stability of the electrode.

In short, the NiO/CNT electrode showed excellent rate performance and good cycling stability, which may be ascribed to the advantages of its unique structure as follows: (1) the rich mesopores can not only make the electrolyte smoothly penetrate to the active materials and reduce the distance of Li ions transport to improve the rate performance, but also accommodate the volume change to ensure the stability of SEI films and the integrity of the electrode; (2) CNTs penetrate and extend out of NiO microsphere to bridge microspheres so as to form long-range conducting networks, which ensures the excellent electronic conductivity of integral electrode; (3)the microsphere assembled with nanoparticles can take the advantage of nanoparticles such as reducing the distance of ions and electrons transport, but can circumvent the limitation of low-dimensional nanoparticles such as their easy aggregation; (4) the hollow structure can further alleviate the strains of volume effect to improve the cycle stability, as well as adsorb Li^+ through its dangle bonds on the surface to

improve the specific capacities; (5) the coated amorphous carbon protect the NiO active material from the direct contact with electrolyte and improve the cycle stability. Due to the combination effect of these factors, this CNTs penetrated hollow structure shows excellent electrochemical properties.

4. Conclusions

In summary, we have demonstrated the preparation and electrochemical properties of NiO hollow microspheres interconnected by MWCNTs. The microspheres consisting of NiO nanoparticles and mesopores, as well as MWCNTs showed significantly improved rate performance and cycle stability in comparison with a porous NiO electrode. The improvement is attributed to the good electrochemical property of NiO microspheres, excellent electric conductivity of MWCNTs, and rich mesopores of the composite electrode.

Acknowledgments

This work was financially supported by the National Natural Science Foundation of China (51572078, 51272073 and 51541203) and Student National SIT Innovation Program. This research was partically supported by the University of Queensland under the Vice-Chancellor's Research and Teaching Fellowship Program(2015000144).

References

[1] P. Poizot, S. Laruelle, S. Grugeon, L. Dupont, J.M. Tarascon, Nature, 407 (2000) 496-499..

[2] J. Wang, N. Yang, H. Tang, Z. Dong, Q. Jin, M. Yang, D. Kisailus, H. Zhao, Z. Tang, D. Wang, Angewandte Chemie International Edition, 52 (2013) 6417-6420.

[3] X. Dong, W. Yuan, Z. Dong, Q. Su, J. Zhang, G. Du, Electrochimica Acta, 92 (2013) 87-92.

[4] X. Li, A. Dhanabalan, K. Bechtold, C. Wang, Electrochemistry Communications, 12 (2010) 1222-1225.

[5] X.H. Huang, J.P. Tu, C.Q. Zhang, F. Zhou, Electrochimica Acta, 55 (2010) 8981-8985.

[6] Z. Bai, Z. Ju, C. Guo, Y. Qian, B. Tang, S. Xiong, Nanoscale, 6 (2014) 3268-3273.

[7] G.P. Kim, S. Park, I. Nam, J. Park, J. Yi, Journal of Power Sources, 237 (2013) 172-177.

[8] X. Liu, S.W. Or, C. Jin, Y. Lv, C. Feng, Y. Sun, Electrochimica Acta, 100 (2013) 140-146.

[9] X. Li, S. Xiong, J. Li, X. Liang, J. Wang, J. Bai, Y. Qian, Chemistry, 19 (2013) 11310-11319.

[10] T. Tao, A.M. Glushenkov, C.F. Zhang, H.Z. Zhang, D. Zhou, Z.P. Guo, H.K. Liu, Q.Y. Chen, H.P. Hu, Y. Chen, Journal of Materials Chemistry, 21 (2011) 9350-9355.

[11] H. Zhang, H. Song, X. Chen, J. Zhou, H. Zhang, Electrochimica Acta, 59 (2012) 160-167.

[12] X. Jia, R. Wang, Z. Chen, H. Yu, F. Wei, Y. Lu, Electrochemistry Communications, 46 (2014) 52-55.

[13] G. Huang, F. Zhang, X. Du, Y. Qin, D. Yin, L. Wang, ACS nano, 9 (2015) 1592-1599..

[14] S.F. Zheng, J.S. Hu, L.S. Zhong, W.G. Song, L.J. Wan, Y.G. Guo, Chemistry of Materials, 20 (2008) 3617-3622.

[15] L. Yang, J. Hu, A. Dong, D. Yang, Electrochimica Acta, 144 (2014) 235-242.

[16] W.W. Liu, C.X. Lu, X.L. Wang, K. Lianga, B.K. Tay, Journal of Materials Chemistry A, 3 (2014) 624-633.

[17] L. Kang, J. Deng, T. Liu, M. Cui, X. Zhang, P. Li, Y. Li, X. Liu, W. Liang, Journal of Power Sources, 275 (2015) 126-135.

[18] J. Cheng, B. Wang, D.C.-M. Park, D.Y. Wu, H. Huang, F. Nie, Chemistry - A European Journal, 19 (2013) 9866-9874.

[19] S. Ko, J. Li, H.S. Yang, S. Park, U. Jeong, Advanced materials, 24 (2012) 4451-4456.

[20] A. Hu, X. Chen, Y. Tang, Q. Tang, L. Yang, S. Zhang, Electrochemistry Communications, 28 (2013) 139-142.

[21] S. Yang, W. Yue, J. Zhu, Y. Ren, X. Yang, Advanced Functional Materials, 23 (2013) 3570–3576.

[22] W. Wei, S. Yang, H. Zhou, I. Lieberwirth, X. Feng, K. Müllen, Advanced materials, 25 (2013) 2909-2914.

[23] D. Cai, D. Li, S. Wang, X. Zhu, W. Yang, S. Zhang, H. Wang, Journal of Alloys and Compounds, 561 (2013) 54-58.

[24] Y. Sun, X. Hu, W. Luo, F. Xia, Y. Huang, Advanced Functional Materials, 23 (2012) 2436-2444.

[25] X. Zhou, Z. Dai, S. Liu, J. Bao, Y.G. Guo, Advanced Materials, 26 (2014) 3943-3949.

[26] X. Zhao, Y. Du, L. Jin, Y. Yang, S. Wu, W. Li, Y. Yu, Y. Zhu, Q. Zhang, Scientific Reports, 5 (2015).

[27] C. Wu, X. Li, W. Li, B. Li, Y. Wang, Y. Wang, M. Xu, L. Xing, Journal of Power Sources, 251 (2014) 85-91.

[28] X. Li, Y. Chen, L. Zhou, Y.W. Mai, H. Huang, Journal of Materials Chemistry A, 2 (2014) 3875-3880.

[29] J.S. Cho, Y.J. Hong, Y.C. Kang, ACS nano, 9 (2015) 4026-4035.

[30] G.V. Lier, C.V. Alsenoy, V.V. Doren, P. Geerlings, Chemical Physics Letters, 326 (2000) 181-185.

[31] P. Zhang, J. Qiu, Z. Zheng, G. Liu, M. Ling, W. Martens, H. Wang, H. Zhao, S. Zhang, Electrochimica Acta, 104 (2013) 41-47.

[32] C.D.L. Casas, W. Li, Journal of Power Sources, 208 (2012) 74-85.

[33] B. Wang, X. Li, B. Luo, X. Zhang, Y. Shang, A. Cao, L. Zhi, ACS applied materials & interfaces, 5 (2013) 6467-6472.

[34] X. Jia, Y. Cheng, Y. Lu, F. Wei, ACS nano, 8 (2014) 9265-9273.

[35] D.Liu, H.F. Wang, X.L. Chen, Journal of Advances in Physical Chemistry, 04 (2015) 24-30.

[36] G. Zhang, T. Feng, C. Zhao, L. Chen, P. Zhang, Y. Wang, C. Gong, Z. Zhang, E. Xie, Applied Surface Science, 311 (2014) 384-390.

[37] S. Xuan, L. Hao, W. Jiang, X. Gong, Y. Hu, Z. Chen, Nanotechnology, 18 (2007) 386-386.

[38] J. Ge, J. Shi, L. Chen, Carbon, 47 (2009) 1192-1195.

[39] M. Ling, J. Qiu, S. Li, H. Zhao, G. Liu, S. Zhang, Journal of Materials Chemistry A, 1 (2013) 11543-11547.

[40] L. Tao, J. Zai, K. Wang, H. Zhang, M. Xu, J. Shen, Y. Su, X. Qian, Journal of Power Sources, 202 (2012) 230-235.

[41] B. Koo, H. Xiong, M.D. Slater, V.B. Prakapenka, M. Balasubramanian, P. Podsiadlo, C.S. Johnson, T. Rajh, E.V. Shevchenko, Nano Letters, 12 (2012) 2429-2435.

[42] P. Ruetschi, R. Giovanoli, Journal of the Electrochemical Society, 135 (1987) 2663-2669.

[43] T. Zhu, J.S. Chen, X.W. Lou, Journal of Materials Chemistry C, 115 (2011) 9814-9820.

[44] S.M. Abbas, S. Ali, N. Ahmad, N. Ali, K.S. Munawar, S.T. Hussain, Electrochimica Acta, 105 (2013) 481-488.

[45] P. Lian, X. Zhu, H. Xiang, Z. Li, W. Yang, H. Wang, Electrochim Acta, Electrochimica Acta, 56 (2010) 834-840.

[46] S.H. Lee, S.H. Yu, J.E. Lee, A. Jin, D.J. Lee, N. Lee, H. Jo, K. Shin, T.Y. Ahn, Y.W. Kim, Nano Letters, 13 (2013) 4249-4256.

[47] S. Grugeon, S. Laruelle, R. Herrera-Urbina, L. Dupont, P. Poizot, J.M. Tarascon, Journal of the Electrochemical Society, 148 (2001) A285-A292.

[48] M. Sasidharan, N. Gunawardhana, C. Senthil, M. Yoshio, Journal of Materials Chemistry A, 2 (2014) 7337.

[49] L. Chu, M. Li, X. Li, Y. Wang, Z. Wan, S. Dou, D. Song, Y. Li, B. Jiang, RSC Adv., 5 (2015) 49765-49770.

[50] J. Bai, X. Li, G. Liu, Y. Qian, S. Xiong, Advanced Functional Materials, 24 (2014) 3012-3020.

[51] G. Zhou, D.W. Wang, F. Li, L. Zhang, N. Li, Z. S. Wu, L. Wen, G. Q. Lu, H. M. Cheng, Chem. Mater., 22(2010) 5306-5313.

[52] M. Zhang, R. Li, X. Chang, C. Xue, X. Gou, Journal of Power Sources, 290 (2015) 25-34.

[53] M. Ling, J. Qiu, S. Li, C. Yan, M.J. Kiefel, G. Liu, S. Zhang, Nano letters, 15 (2015) 4440-4447.

Figure Captions

Fig.1 (A) The XRD patterns of (a) NiO/CNT composites; (b) NiO; (c) functionalized CNTs; (B) the TG curve of the NiO/CNTs composites.

Fig.2 (a) SEM image of NiO/CNTs hollow microspheres at low-magnification image; (b) SEM image of NiO/CNTs hollow microspheres at high-magnification image; (c) TEM image of NiO/CNTs hollow microspheres; (d) HRTEM images of NiO/CNTs hollow microspheres the inset in (d) is its SAED pattern.

Fig.3 The FT-IR spectra of (a) functionalized CNTs; (b) NiO; (c) NiO/CNTs composites.

Fig.4 (a) The N_2 adsorption-desorption isotherms of NiO/CNTs hollow microspheres and the inset in (a) is its pore-size distribution; (b) The N_2 adsorption-desorption isotherms of NiO hollow microspheres and the inset in (b) is its pore-size distribution.

Fig.5 Schematic illustration of the procedure for preparing NiO/CNTs hollow microspheres.

Fig. 6 The cycle voltammograms between 0.01V and 3 V at a scan rate of 0.1 mV/s

(a) NiO/CNTs; (b) NiO.

Fig. 7 (a) The discharge/charge voltage profiles of NiO/CNTs; (b) rate performance at various current densities between 0.1 and 5C; (c) EIS profiles of pure NiO and NiO/CNTs composites electrodes; the insert is the room part at high frequency region and (d) cycling performance curves of NiO/CNTs composites and pure NiO electrodes at the rate 1C

Fig.8 The SEM image of porous NiO hollow microspheres after the 100^{th} charge/discharge cycle at the rate 1C

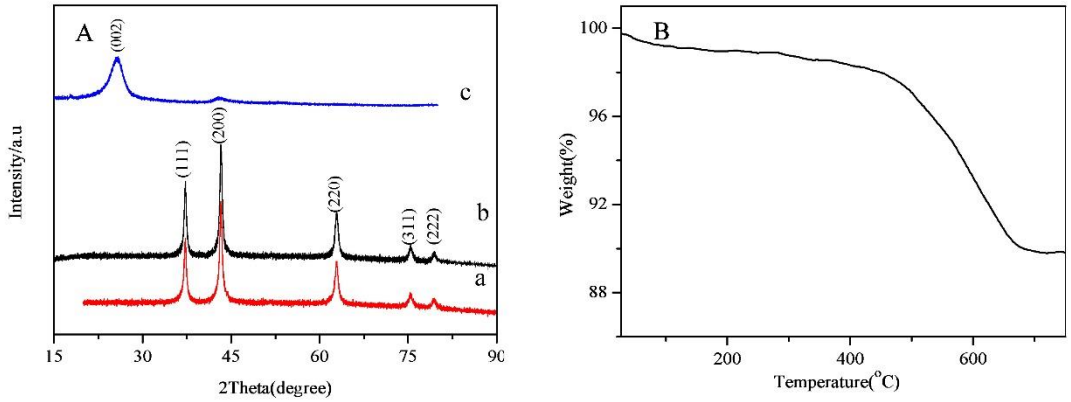

Fig. 1

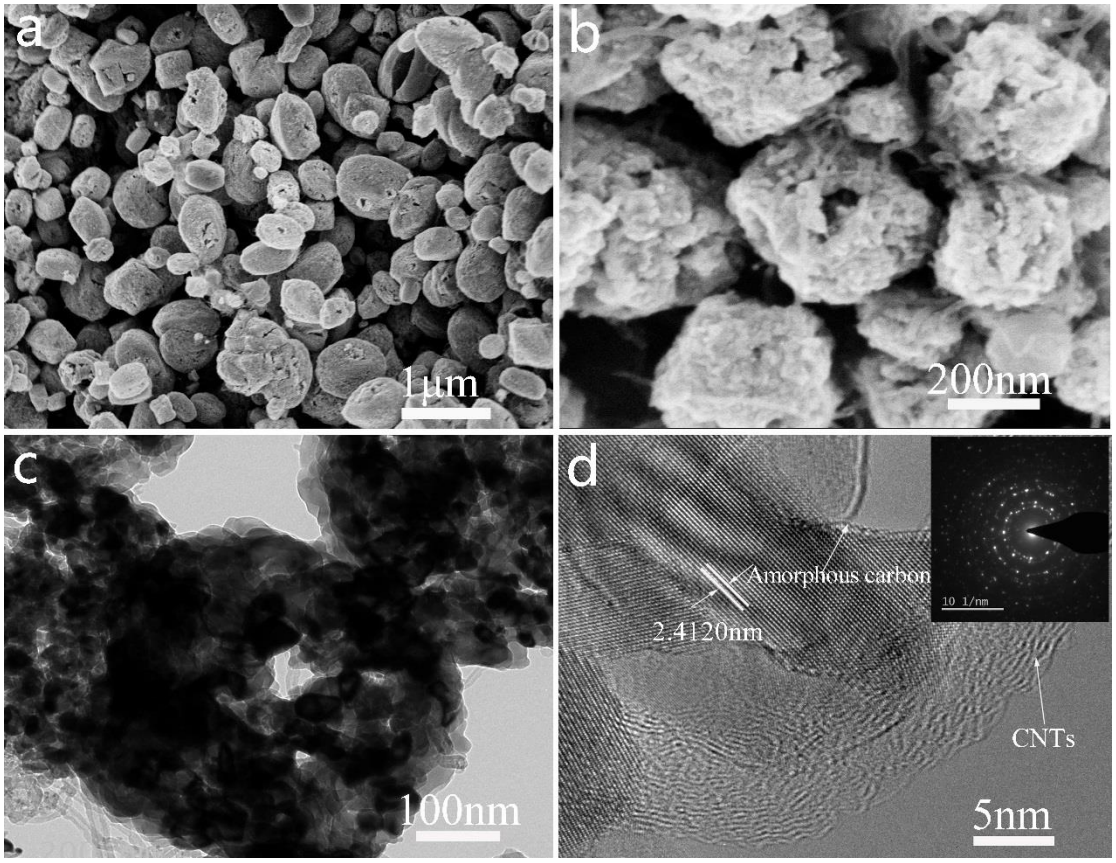

Fig.2

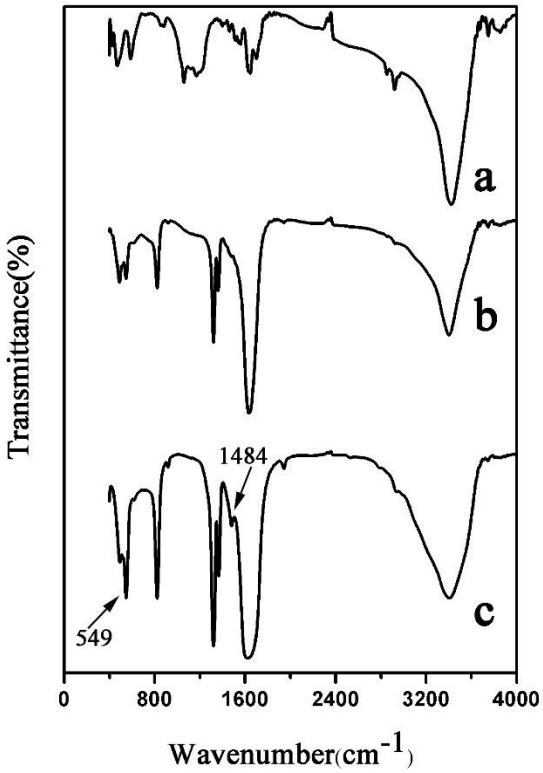

Fig. 3

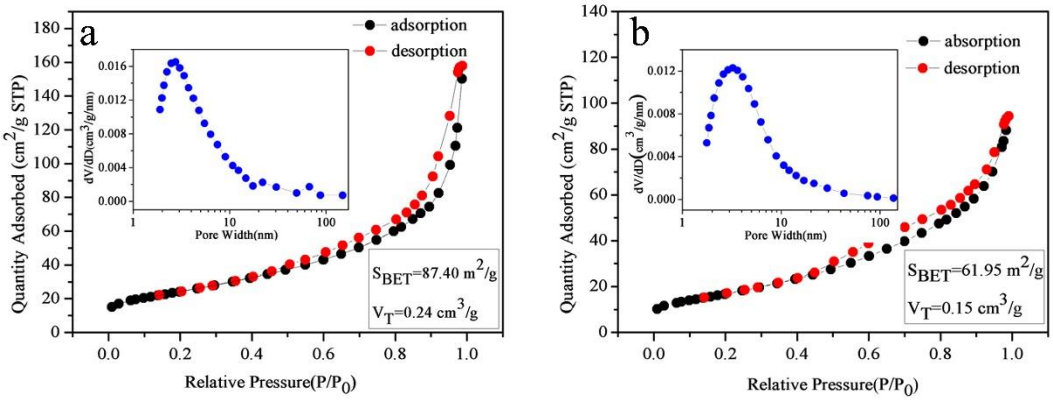

Fig. 4

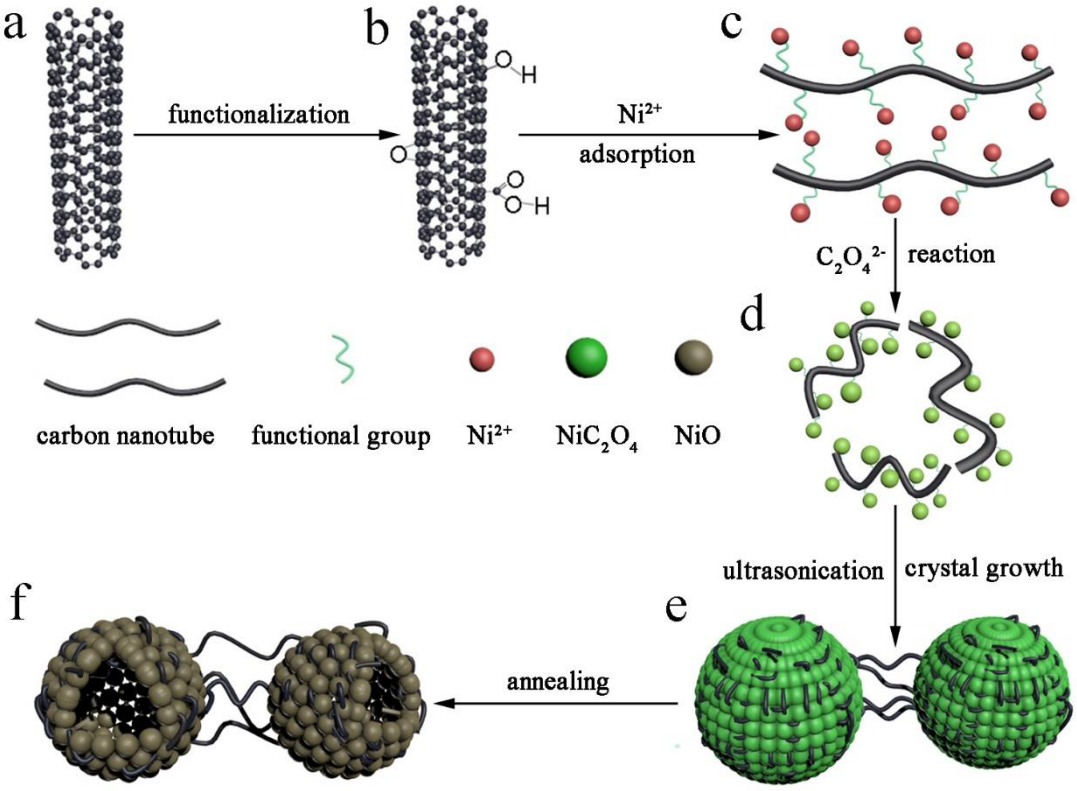

Fig. 5

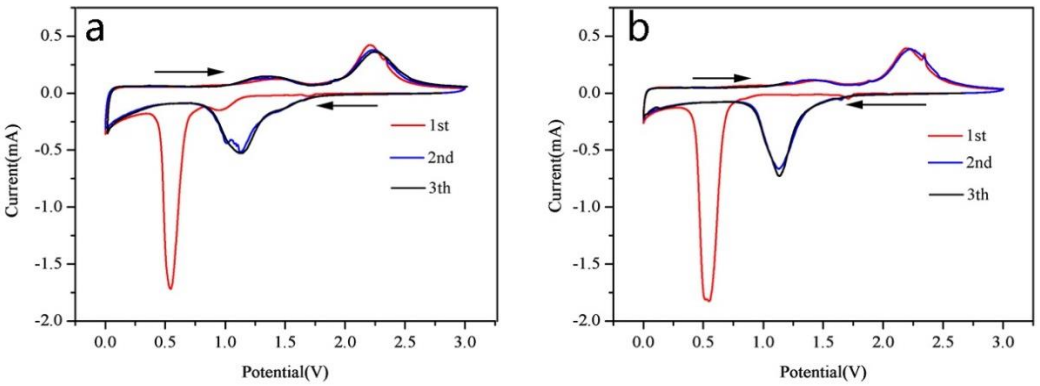

Fig. 6

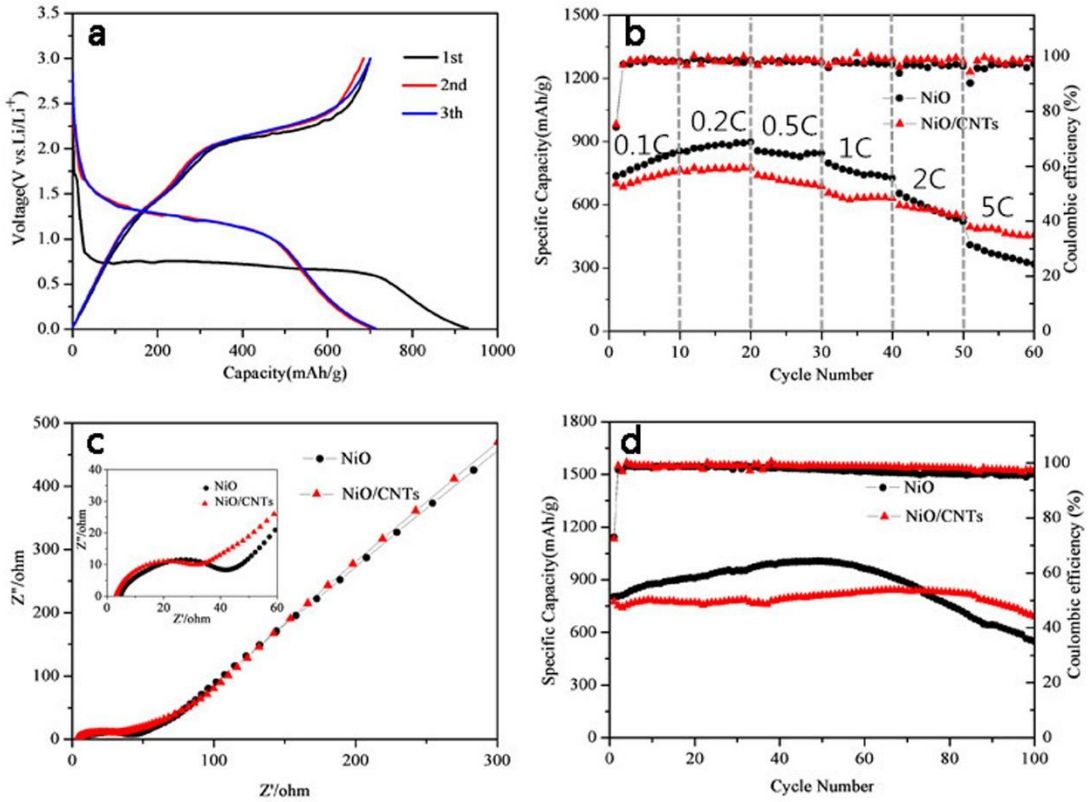

Fig. 7

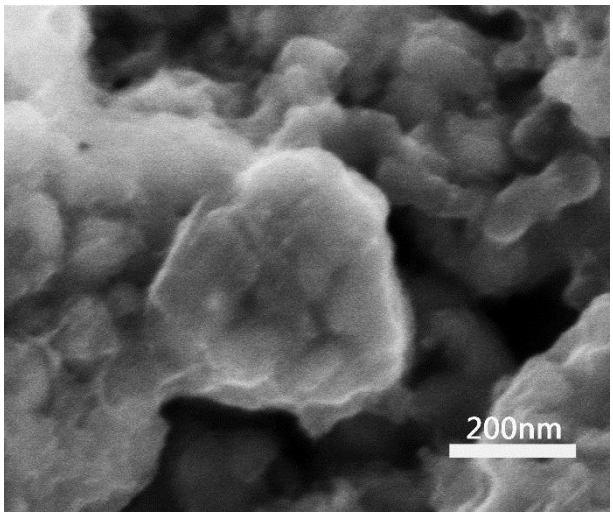

Fig. 8